

Article

Determining the Stability of a Mobile Manipulator for the Transport and Assembly of Arches in the Yielding Arch Support

Krzysztof Krauze¹, Kamil Mucha^{1,*}, Tomasz Wydro¹, Ryszard Klempka², Andrzej Kutnik³, Waldemar Hałas³ and Piotr Ruda³

¹ Faculty of Mechanical Engineering and Robotics, AGH University of Science and Technology, al. Mickiewicza 30, 30-059 Kraków, Poland; krauze@agh.edu.pl (K.K.); wydro@agh.edu.pl (T.W.)

² Faculty of Electrical Engineering, Automatics, Computer Science and Biomedical Engineering, AGH University of Science and Technology, al. Mickiewicza 30, 30-059 Kraków, Poland; klempka@agh.edu.pl

³ FAMA Sp. z o.o., ul. Przemysłowa 1, 83-140 Gniew, Poland; andrzej.kutnik@fama-gniew.com (A.K.); waldemar.halas@fama-gniew.pl (W.H.); piotr.ruda@fama-gniew.com (P.R.)

* Correspondence: kmucha@agh.edu.pl

Abstract: The yielding arch support is transported and installed in the face with the use of auxiliary machines. These activities in underground mining cause many problems, which have as yet not been solved. Currently, transport and assembly are carried out manually, using the roadheader and suspended rail, or various types of mounting platforms. The analysis of the structure of the existing solutions resulted in the development of an original structure that met the requirements of Polish mines. Developed jointly by FAMA Sp. z o.o. and the AGH University of Science and Technology in Krakow, Poland, the mining modular transport and assembly unit (MZT-M) will enable the transport and assembly of support arches in the mining face. Additionally, it can also be used to reload works, which is related to the work ergonomics in underground coal mining, which is the main energy resource in Poland. The most important problem to be solved in the case of this manipulator, due to the limited space in the excavation, is how to ensure its stability during various phases of its operation. Therefore, analyses were carried out to find a solution, which resulted in determining specific conditions and design requirements related to the operation of this manipulator.

Keywords: coal mining; transport and assembly manipulator; stability; safety; work ergonomics



Citation: Krauze, K.; Mucha, K.; Wydro, T.; Klempka, R.; Kutnik, A.; Hałas, W.; Ruda, P. Determining the Stability of a Mobile Manipulator for the Transport and Assembly of Arches in the Yielding Arch Support. *Energies* **2022**, *15*, 3170. <https://doi.org/10.3390/en15093170>

Academic Editors: Manoj Khandelwal and Krzysztof Skrzypkowski

Received: 18 March 2022

Accepted: 21 April 2022

Published: 26 April 2022

Publisher's Note: MDPI stays neutral with regard to jurisdictional claims in published maps and institutional affiliations.



Copyright: © 2022 by the authors. Licensee MDPI, Basel, Switzerland. This article is an open access article distributed under the terms and conditions of the Creative Commons Attribution (CC BY) license (<https://creativecommons.org/licenses/by/4.0/>).

1. Introduction

In hard coal mines, one of the key processes is tunnelling. During tunnelling and later during the exploitation of such an excavation, it is deformed due to the pressure of the rock mass [1,2]. The floor may be deformed [3,4], but the more serious danger is caused by the roof deformation [5–7]. Hence, various types of support for tunnels are used [8–11], but the most commonly used in hard coal mines are yielding arch support frames [12–14].

The use of yielding arch support frames in galleries of underground mines involves installing their elements in the face using a roadheader [15,16]. For this purpose, apart from the aforementioned roadheader, a suspended monorail [17] and moving equipment are used. It is easy to notice that this process, i.e., the transport of support arches and other elements of the support, the lining, as well as the assembly itself, is performed manually. Delivering the support elements to the face is particularly cumbersome and requires a lot of physical effort. Hence, an idea arose to use a device enabling the transfer of elements of the support frame from the place of their storage to the face, in front of the roadheader, and to deliver them to the place of assembly [18–20].

The current solutions do not enable one to perform the above-mentioned functions due to the dimensions of the excavation. This is clearly visible in the attached photo (Figure 1), where the manipulator is attached to the platform. Examples of such solutions are GTA [21]

and Deilmann–Haniel Mining Systems GmbH [22] platforms. However, in this situation, it is not possible for the platform to ride over the roadheader (Figure 2).

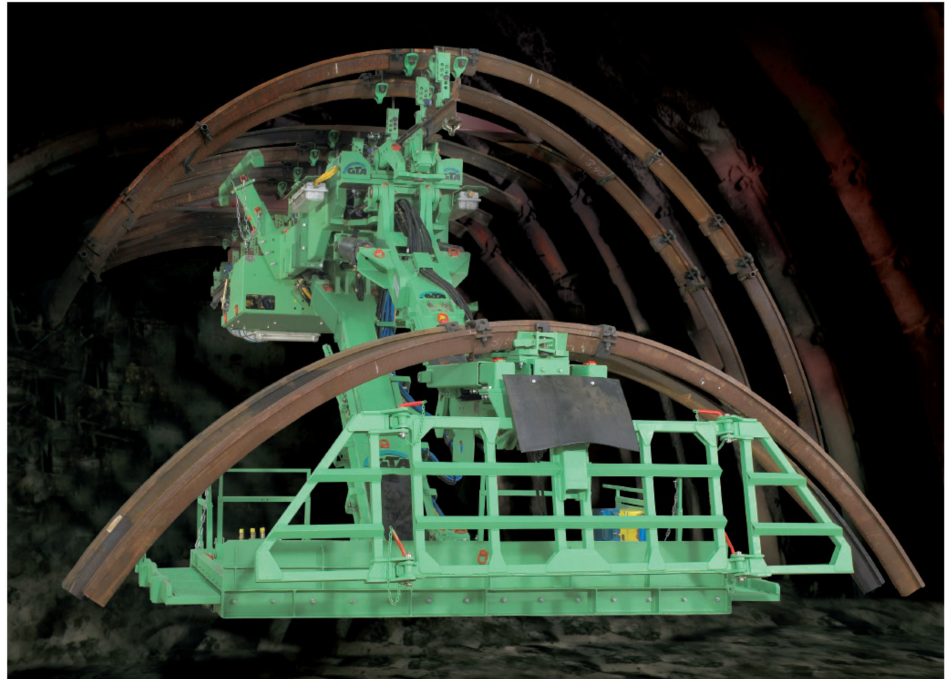


Figure 1. Roadway Support Machine AMG 5000 produced by GTA [21].



Figure 2. View of the mining face of a gallery drilled with a roadheader.

A conceptual diagram of the manipulator, consisting of a boom mounted on one runway beam with a stabilizing foot and a hydraulic power unit, and consisting separately of a haulage drive (haulage unit) moving along the suspended monorail track, is shown in Figure 3a [19,20].

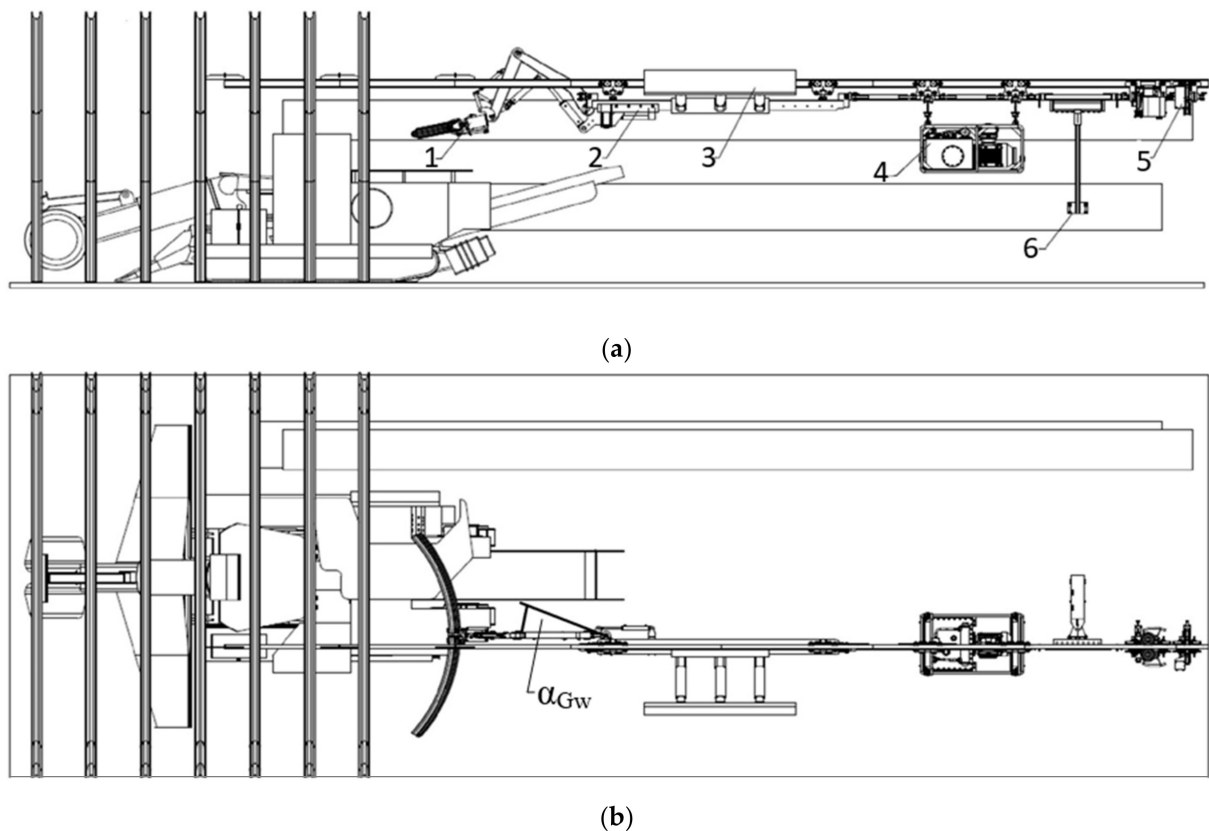


Figure 3. Diagram of the MZT-M in a gallery system with the arch in the transport position: (a) side view, (b) top view: 1—boom, 2—beam, 3—support slide, 4—hydraulic power unit, 5—CHM-15 tractor, 6—control panel [19,20].

A characteristic feature of this solution is the asymmetrical mounting of the suspended monorail in the gallery and the need to stabilize (balance) the modular transport and assembly unit (MZT-M) during the transport of support elements, whereas the manipulator can only be operated when the stabilizing foot is unfolded.

Bearing in mind the above, the following assumptions were formulated:

- the manipulator with a boom and its drive mounted on one monorail with a useful weight of up to 440 kg or without it in the transport position (boom raised, folded, twisted) can be moved without the possibility of maneuvering at the same time only when the stabilizing foot is folded;
- the maneuvering of the boom itself, with or without a load, is possible only after stoppage, with the use of a stabilizing foot stretched against the yielding support arches.

Therefore, the manipulator balancing process was performed for a transport position with a permissible boom rotation with an angle $\alpha_{Gw} \leq 30^\circ$ (Figures 3b and 4). The model of the boom with its individual elements marked is shown in Figure 5.

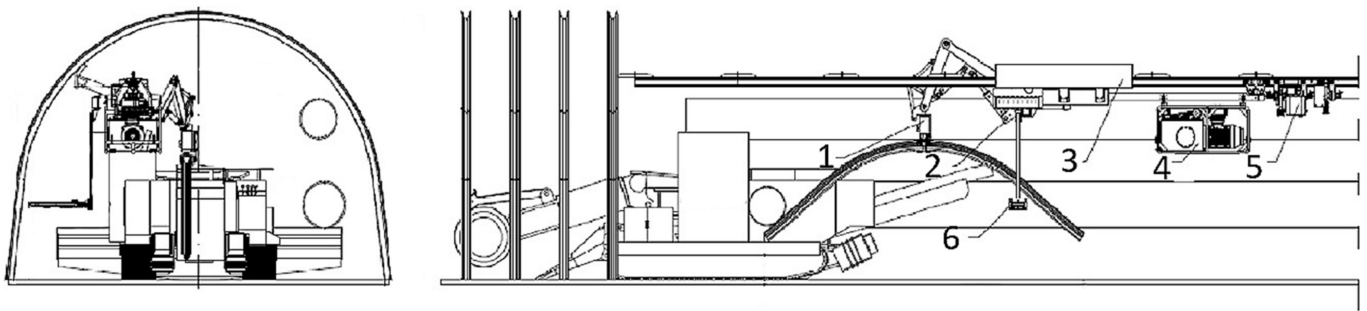


Figure 4. Diagram of the MZT-M in the transport position: 1—boom, 2—beam, 3—support slide, 4—hydraulic power unit, 5—CHM-15 tractor, 6—control panel.

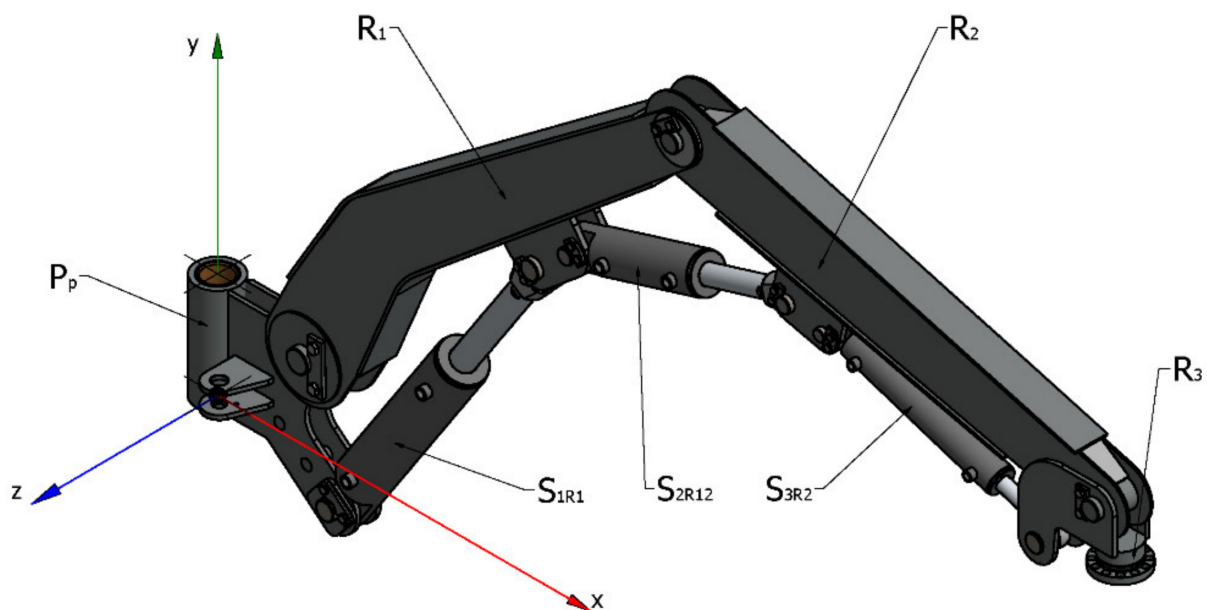


Figure 5. Boom model: P_p —vertical joint, R_1 —first arm, R_2 —second arm, R_3 —third arm with a handle, S_{1R1} —first arm cylinder, S_{2R12} —second arm cylinder, S_{3R2} —third arm cylinder.

The article's main objective is to present the process of analytically determining the stability of the manipulator during various phases of its operation and to determine the counterweight mass for the boom in the transport position. A solution was searched for, resulting in specific conditions and design requirements related to the operation of this manipulator being obtained and specified.

2. Analytical Model of the Manipulator and Methodology for Determining Its Stability

As mentioned before, the aim of this article was to determine the counterweight for the boom in the transport position. Therefore, the boom model shown in Figure 5 was adapted, with the boom elements being marked in Figures 6 and 7.

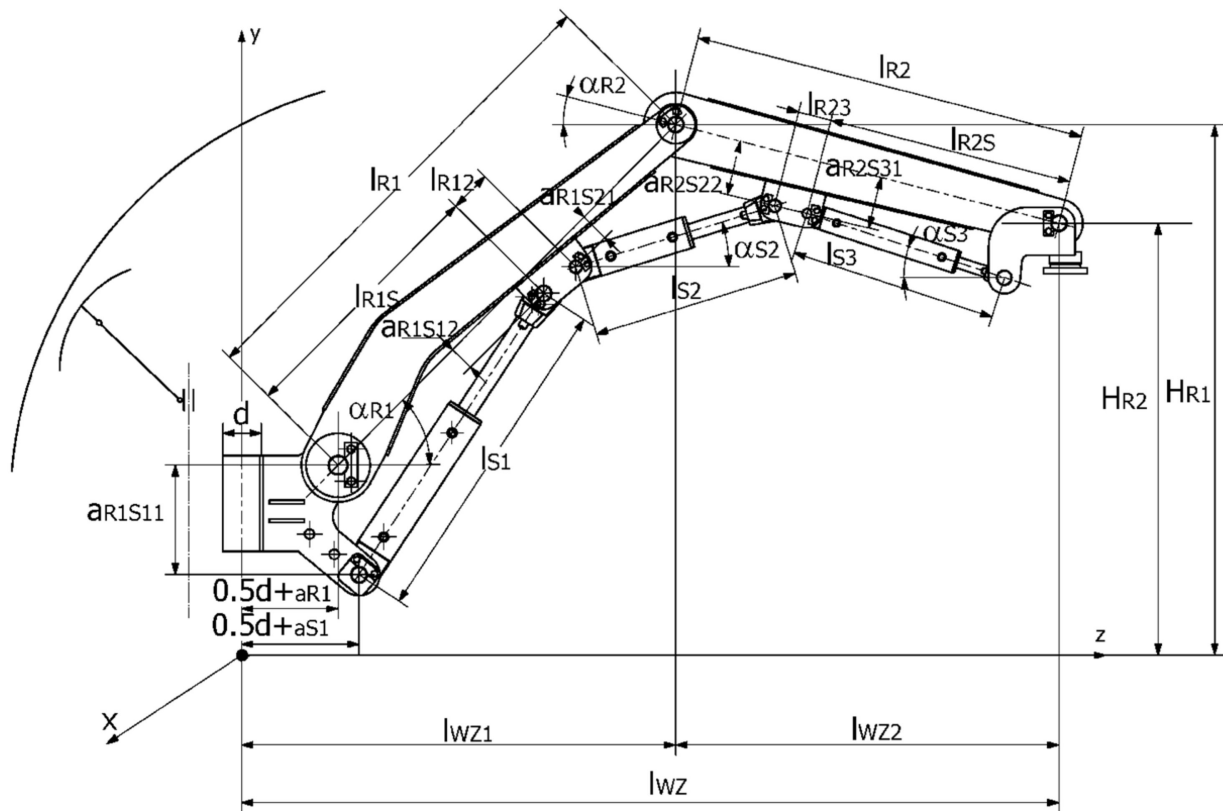


Figure 6. Diagram of the boom with marked dimensions.

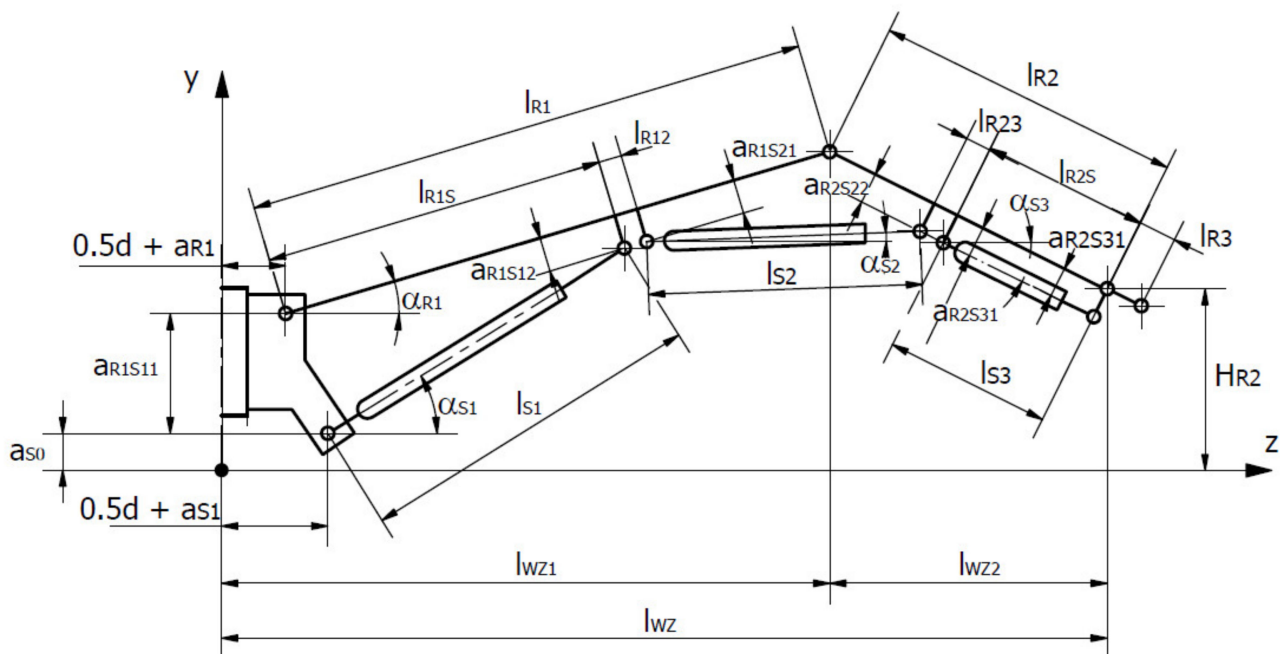


Figure 7. Analytical model of the boom for determining stability.

Based on the analytical model (Figure 7), the structure and kinematics of the R1 arm were considered (Figures 5 and 8). Bearing in mind the diagram (Figure 8), the dependencies that allowed one to describe the quantities that were important for the assessment of the arm's stability as a function of the construction parameters were determined.

$$\alpha_{R1} = \alpha_{R11} + \alpha_{R12} \quad (1)$$

$$\alpha_{R11} = \arctg\left(\frac{a_{R1S12}}{l_{R1S}}\right) \quad (2)$$

$$\alpha_{R12} = \arccos\left[\frac{\left[(a_{S1} - a_{R1})^2 + a_{R1S11}^2 + (l_{R1S} \cdot \cos \alpha_{R11}^{-1})^2\right] - l_{S1}^2}{2 \cdot l_{R1S} \cdot \cos \alpha_{R11}^{-1} \cdot \sqrt{(a_{S1} - a_{R1})^2 + a_{R1S11}^2}}\right] - \arctg\left(\frac{a_{R1S11}}{a_{S1} - a_{R1}}\right) \quad (3)$$

$$\alpha_{S1} = 90^\circ + \arctg\left(\frac{a_{S1} - a_{R1}}{a_{R1S11}}\right) - \arccos\left[\frac{a_{R1S11}^2 + (a_{S1} - a_{R1})^2 - l_{R1S}^2 \cdot \cos \alpha_{R11}^{-1} + l_{S1}^2}{2 \cdot l_{S1} \cdot \sqrt{(a_{S1} - a_{R1})^2 + a_{R1S11}^2}}\right] \quad (4)$$

$$H_{R1} = a_{S0} + a_{R1S11} + l_{R1} \cdot \sin \alpha_{R1} \quad (5)$$

$$l_{WZ1} = 0.5 \cdot d + a_{R1} + l_{R1} \cdot \cos \alpha_{R1} \quad (6)$$

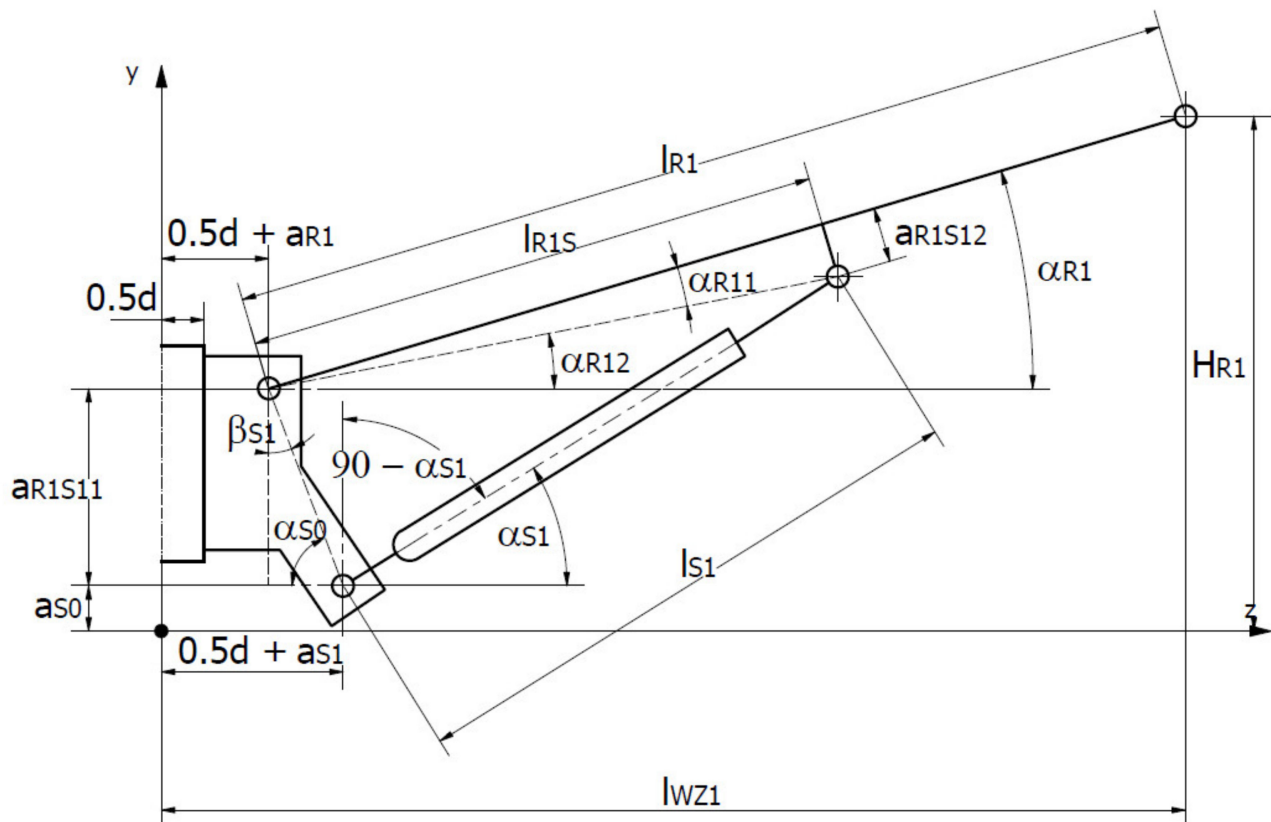


Figure 8. Computational diagram of the R1 arm.

The same was done for the R2 arm, whose computational diagram is presented in Figure 9.

$$\alpha_{R21} = \arctg\left[\frac{a_{R2S22}}{l_{R2} - (l_{R2S} + l_{R23})}\right] \quad (7)$$

$$\alpha_{R10} = \arctg\left[\frac{a_{R1S21}}{l_{R1} - (l_{R1S} + l_{R12})}\right] \quad (8)$$

$$A = \frac{l_{R2} - (l_{R2S} + l_{R23})}{\cos \alpha_{R21}} \quad (9)$$

$$B = \frac{l_{R1} - (l_{R1S} + l_{R12})}{\cos \alpha_{R10}} \quad (10)$$

$$\alpha_{R1R2} = \arccos\left(\frac{A^2 + B^2 - l_{S2}^2}{2 \cdot A \cdot B}\right) \quad (11)$$

$$\alpha_{R2} = 180^\circ - (\alpha_{R21} + \alpha_{R10} + \alpha_{R1} + \alpha_{R1R2}) \quad (12)$$

$$\alpha_{S2} = \alpha_{R10} + \alpha_{R1} - \alpha_{R1S1} \quad (13)$$

$$\alpha_{R1S1} = \arccos\left(\frac{B^2 + l_{S2}^2 - A^2}{2 \cdot l_{S2} \cdot B}\right) \quad (14)$$

$$H_{R2} = H_{R1} - l_{R2} \cdot \sin \alpha_{R2} \quad (15)$$

$$l_{WZ2} = l_{R2} \cdot \cos \alpha_{R2} \quad (16)$$

$$l_{S1} = l_{S1min} + \Delta S_{S1} \quad (17)$$

$$l_{S2} = l_{S2min} + \Delta S_{S2} \quad (18)$$

$$l_{S3} = l_{S3min} + \Delta S_{S3} \quad (19)$$

$$l_{WZ} = l_{WZ1} + l_{WZ2} \quad (20)$$

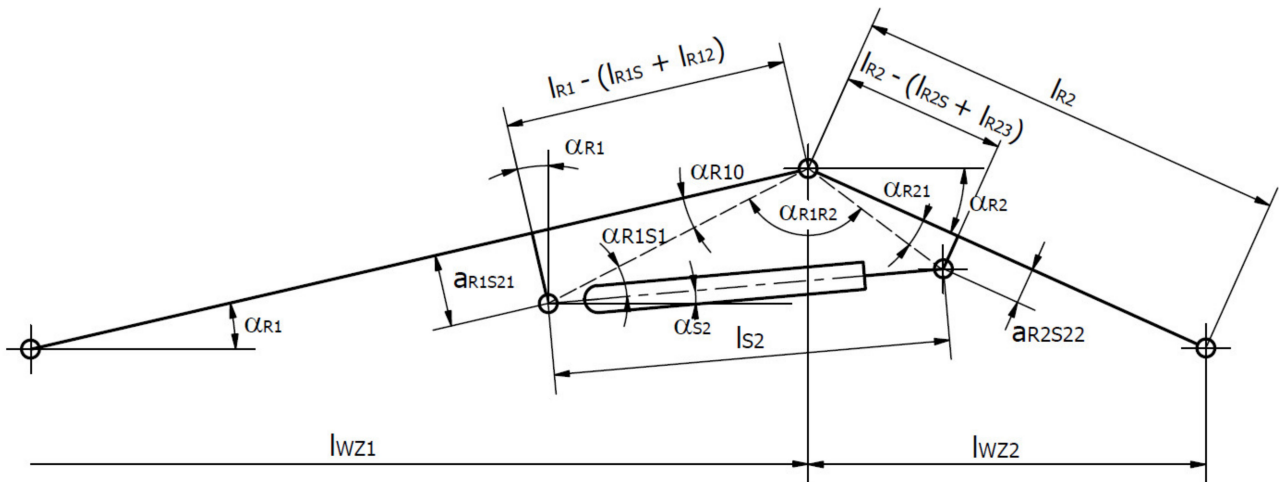


Figure 9. Computational diagram of the R2 arm.

The computational diagram of the R2 arm and more specifically its end, consisting of a gripping part that is moved by the S3 actuator, is presented in Figure 10.

$$\alpha_{R22} = \arctg\left(\frac{a_{R2S31}}{l_{R2S}}\right) \quad (21)$$

$$\alpha_{R2S31} = \arccos\left[\frac{l_{S3}^2 + (l_{R2S} \cdot \cos \alpha_{R22}^{-1})^2 - a_{R2S32}^2}{2 \cdot l_{S3} \cdot l_{R2S} \cdot \cos \alpha_{R22}^{-1}}\right] \quad (22)$$

$$\alpha_{S3} = \alpha_{R2} - \alpha_{R22} + \alpha_{R2S31} \quad (23)$$

$$\alpha_{R2S32} = \arccos\left[\frac{(l_{R2S} \cdot \cos \alpha_{R22}^{-1})^2 + a_{R2S32}^2 - l_{S3}^2}{2 \cdot l_{R2S} \cdot \cos \alpha_{R22}^{-1} \cdot \alpha_{R2S32}}\right] \quad (24)$$

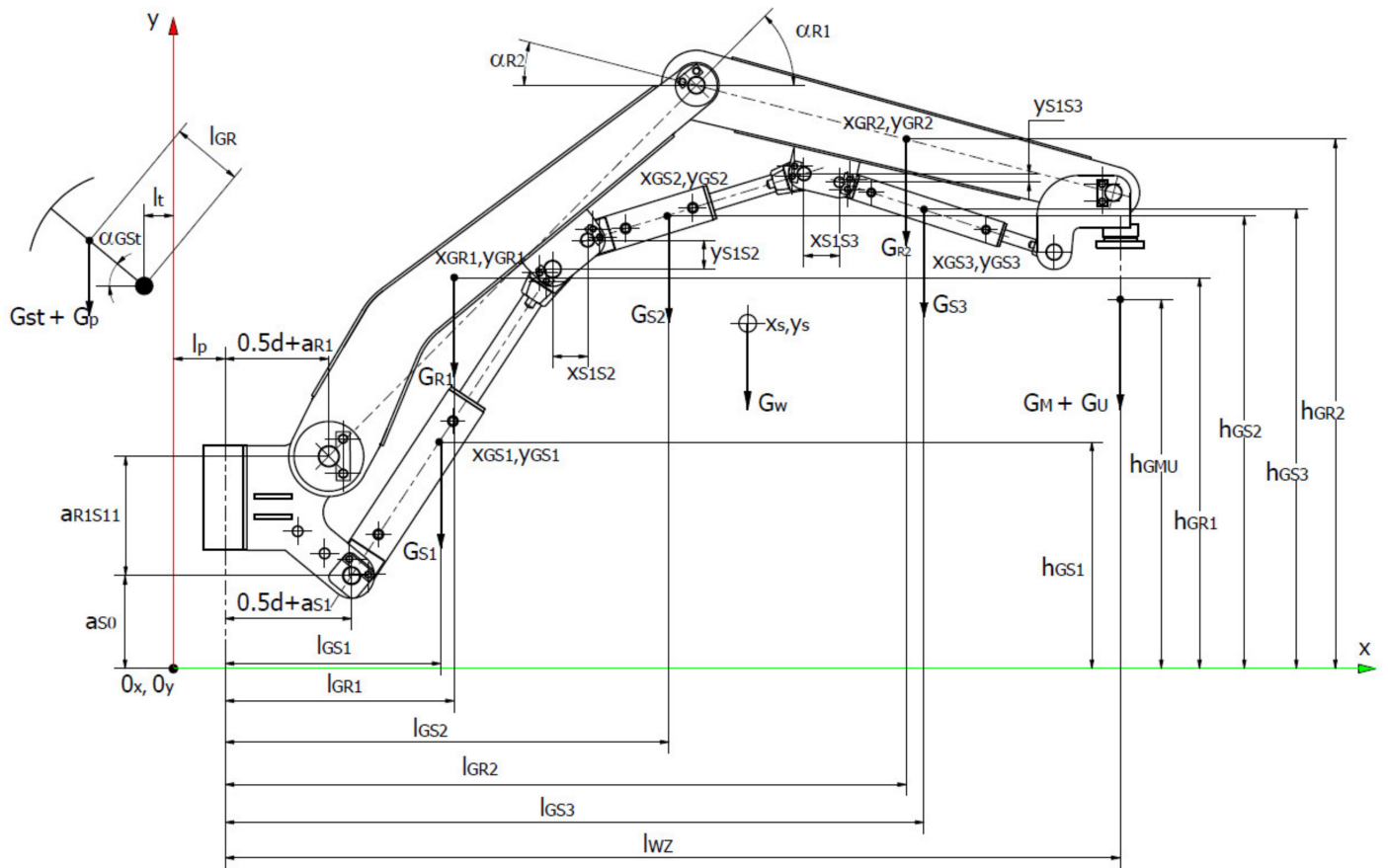


Figure 11. Diagram of the boom for determining the resultant of the center of mass x_s and y_s .

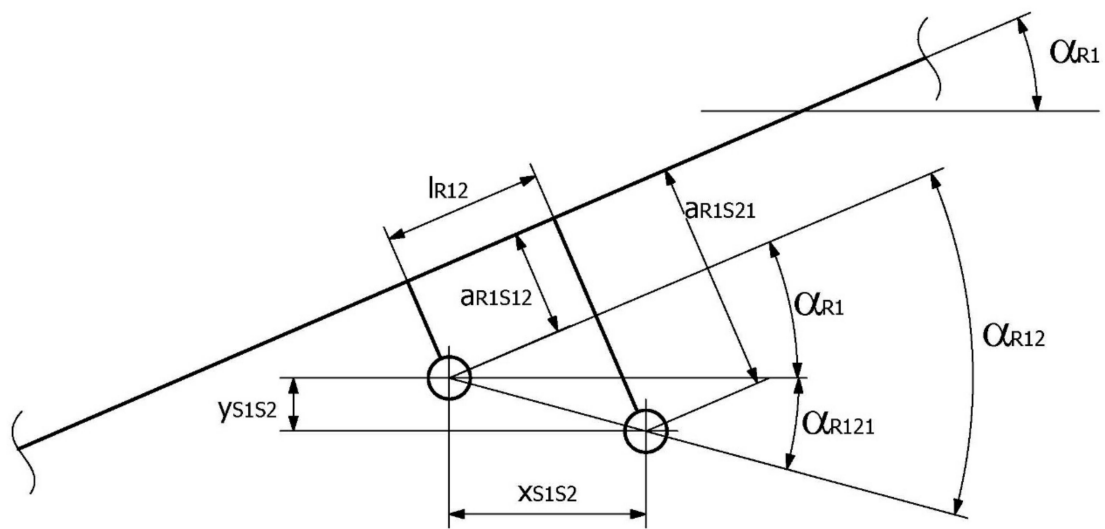


Figure 12. Diagram of the S1 and S2 actuators' mounting.

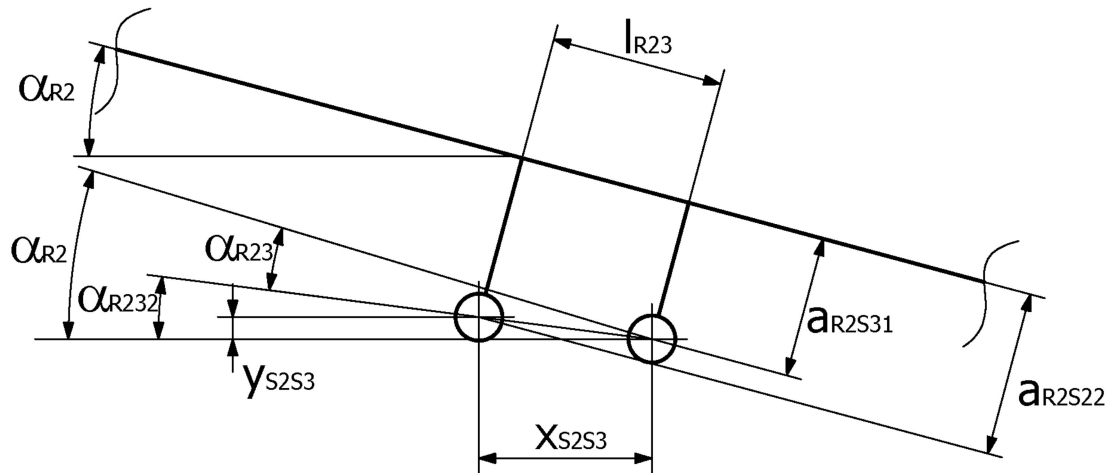


Figure 13. Diagram of the mounting of the S2 and S3 actuators.

G_W —resultant mass (weight), kg
 G_{S1} —mass (weight) of the first actuator, kg
 G_{R1} —mass (weight) of the first arm, kg
 G_{S2} —mass (weight) of the second actuator, kg
 G_{R2} —mass (weight) of the second arm, kg
 G_{S3} —mass (weight) of the third actuator, kg
 G_M —mass (weight) of the gripping part, kg
 G_U —useful mass (weight) (support arch), kg.

$$l_{GS1} = 0.5 \cdot d + a_{S1} + x_{GS1} \cdot \cos \alpha_{S1} + l_p \quad (30)$$

$$l_{GR1} = 0.5 \cdot d + a_{R1} + x_{GR1} \cdot \cos \alpha_{R1} + l_p \quad (31)$$

$$l_{GS2} = 0.5 \cdot d + a_{S1} + x_{GS2} \cdot \cos \alpha_{S2} + l_p + x_{S1S2} + l_{S1} \cdot \cos \alpha_{S1} \quad (32)$$

$$l_{GR2} = x_{GR2} \cdot \cos \alpha_{R2} + l_p + l_{WZ1} \quad (33)$$

$$\alpha_{R12P} = \arctg \left(\frac{a_{R1S21} - a_{R1S12}}{l_{R12}} \right) \quad (34)$$

$$\alpha_{R121} = \alpha_{R12P} - \alpha_{R1} \quad (35)$$

$$\Delta l_{R12} = l_{R12} \cdot \cos \alpha_{R12}^{-1} \quad (36)$$

$$x_{S1S2} = \Delta l_{R12} \cdot \cos \alpha_{R121} \quad (37)$$

$$y_{S1S2} = \Delta l_{R12} \cdot \sin \alpha_{R121} \quad (38)$$

$$\alpha_{R23} = \arctg \left(\frac{a_{R2S22} - a_{R2S31}}{l_{R23}} \right) \quad (39)$$

$$\alpha_{R232} = \alpha_{R2} - \alpha_{R23} \quad (40)$$

$$\Delta l_{R23} = l_{R23} \cdot \cos \alpha_{R23}^{-1} \quad (41)$$

$$x_{S2S3} = \Delta l_{R23} \cdot \cos \alpha_{R232} \quad (42)$$

$$y_{S2S3} = \Delta l_{R23} \cdot \sin \alpha_{R232} \quad (43)$$

$$l_{GS3} = 0.5 \cdot d + a_{S1} + l_p + l_{S1} \cdot \cos \alpha_{S1} + x_{S1S2} + l_{S2} \cdot \cos \alpha_{S2} + x_{S2S3} + x_{GS3} \cdot \cos \alpha_{S3} \quad (44)$$

$$x_s = \frac{G_{S1} \cdot l_{GS1} + G_{R1} \cdot l_{GR1} + G_{S2} \cdot l_{GS2} + G_{R2} \cdot l_{GR2} + G_{S3} \cdot l_{GS3} + (G_M + G_U) \cdot (l_{WZ} + l_{R3X})}{G_{S1} + G_{R1} + G_{S2} + G_{R2} + G_{S3} + G_M + G_U} \quad (45)$$

$$h_{GS1} = a_{S0} + x_{GS1} \cdot \sin \alpha_{S1} \quad (46)$$

$$h_{GR1} = a_{S0} + a_{R1S11} + x_{GR1} \cdot \sin \alpha_{R1} \tag{47}$$

$$h_{GS2} = a_{S0} + l_{S1} \cdot \sin \alpha_{S1} + y_{S1S2} + x_{GS2} \cdot \sin \alpha_{S2} \tag{48}$$

$$h_{GR2} = H_{R1} - x_{GR2} \cdot \sin \alpha_{R2} \tag{49}$$

$$h_{GS3} = a_{S0} + l_{S1} \cdot \sin \alpha_{S1} + y_{S1S2} + l_{S2} \cdot \sin \alpha_{S2} + y_{S2S3} - x_{GS3} \cdot \sin \alpha_{S3} \tag{50}$$

$$h_{GMU} = H_{R2} - l_{R3Y} \tag{51}$$

$$y_s = \frac{G_{S1} \cdot h_{GS1} + G_{R1} \cdot h_{GR1} + G_{S2} \cdot h_{GS2} + G_{R2} \cdot h_{GR2} + G_{S3} \cdot h_{GS3} + (G_M + G_U) \cdot h_{GMU}}{G_{S1} + G_{R1} + G_{S2} + G_{R2} + G_{S3} + G_M + G_U} \tag{52}$$

The location of the center of the entire boom (x_s, y_s) and its resultant mass G_w allows one to determine the counterbalance weight G_{st} (stabilizing foot) for the variant of the manipulator's ride with the support arches. In such a case, it is required for the stabilizing foot not to be in contact with the already installed arch or arches of the support (Figure 14).

$$G_w \cdot x_{st} = G_{st} \cdot l_{Gst} \tag{53}$$

$$l_{Gst} = l_{GS1} \cdot \cos \alpha_{GS1} + l_t \tag{54}$$

where:

G_{st} —mass (weight) of the stabilizing foot, kg

l_{GS1} —length of the arm of the stabilizing foot, m

For the transport position, the value of α_{GW} cannot be greater than 30° , and then:

$$x_{st} = x_s \cdot \sin \alpha_{GW} \tag{55}$$

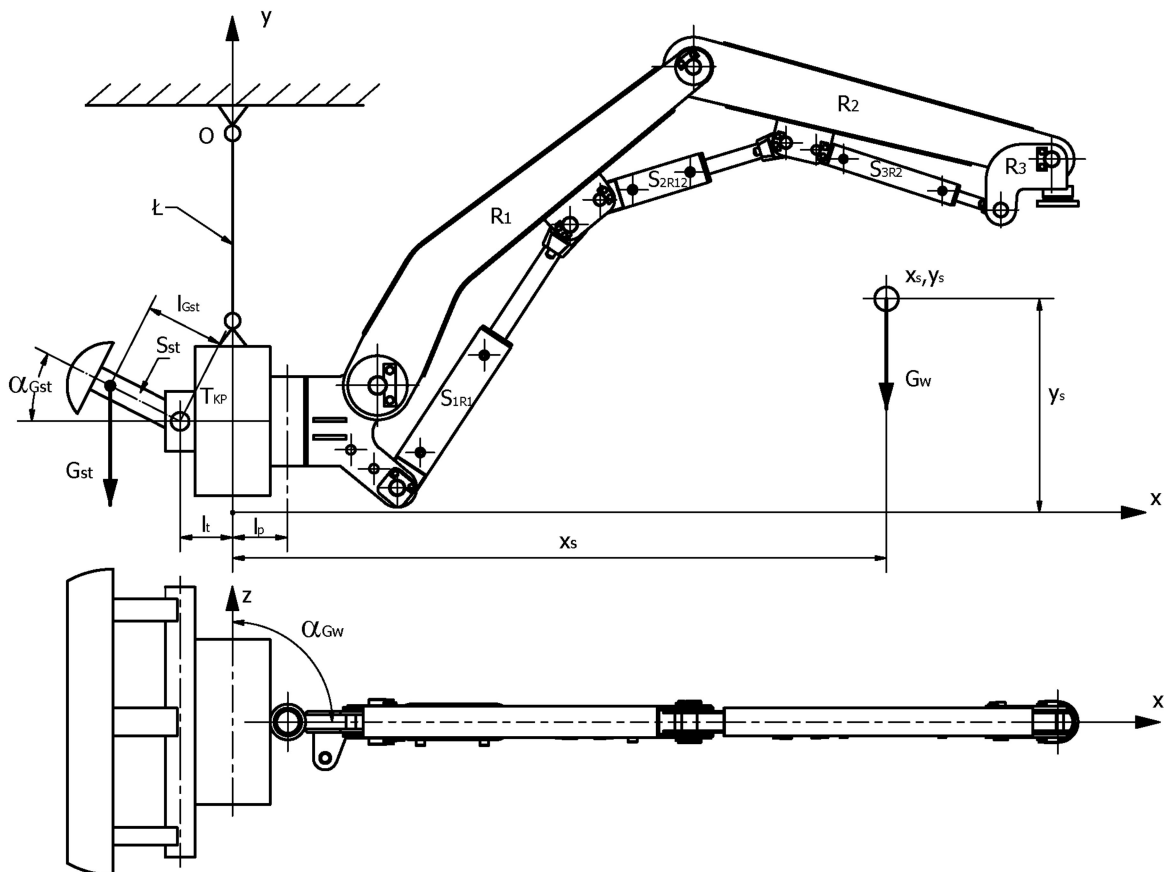


Figure 14. Diagram of the manipulator in the transport position.

Therefore, taking into account the dependencies of Equations (53)–(55), we obtain the following Equation (56), where:

$$G_{St} = \frac{G_W \cdot x_{St}}{l_{GSst}} = G_W \cdot \frac{x_S \cdot \sin \alpha_{GW}}{l_{GSst} \cdot \cos \alpha_{GSst} + l_t} \quad (56)$$

It is equally important to determine the load on the trolleys of the transport beam (points A and B), a simplified diagram of which is shown in Figure 15. Then, the beam is loaded with an additional mass (weight) with the G_z hydraulic power unit and G_n drive.

$$\begin{aligned} l_1 + l_2 + l_3 + l_4 &= 1 \\ \sum P_{iz} &= 0 \rightarrow R_{AZ} = 0 \\ \sum P_{iy} &= 0 \rightarrow -G_z - G_n - G_{st} + R_{BY} - G_w + R_{AY} = 0 \\ R_{AY} &= G_z + G_n + G_{st} + G_w - R_{BY} \end{aligned} \quad (57)$$

$$\begin{aligned} \sum M_{iA} &= 0 \rightarrow -(G_z + G_n) \cdot l_1 - G_{st} \cdot (l_1 + l_2) + R_{BY} \cdot (l_1 + l_2 + l_3) - G_w \cdot (l_1 + l_2 + l_3 + l_4) \\ R_{BY} &= [(G_z + G_n) \cdot l_1 + G_{st} \cdot (l_1 + l_2) + G_w \cdot (l_1 + l_2 + l_3 + l_4)] \cdot (l_1 + l_2 + l_3)^{-1} \end{aligned} \quad (58)$$

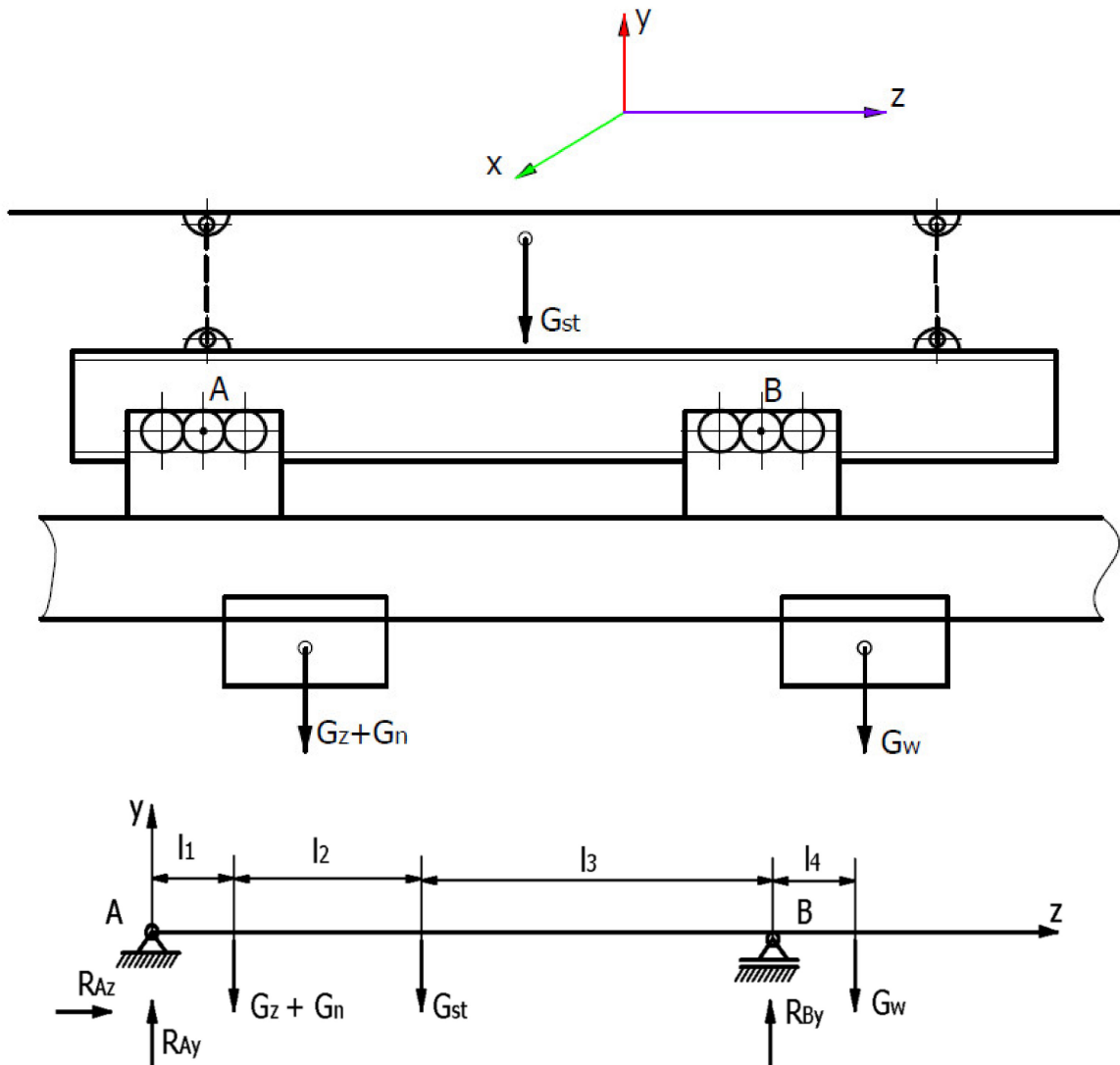


Figure 15. Simplified diagram of the transport beam loading.

3. Calculation Results and Their Analysis

The previously described manipulator model, especially the one dedicated to the transport and assembly of the arch support, was used to develop a preliminary design and, next, a basic design and technical documentation used to create a real object (Figure 16). At the same time, as previously mentioned, data (design parameters) was obtained on the basis of the technical documentation so as to determine the manipulator's stability, especially in the transport position (no contact of the stabilizing foot with the excavation sidewall or with the support elements). It is then important to determine the counterbalance weight, so that the manipulator can move along the excavation axis without the stabilizing foot coming into contact with the sidewall, in the case of movement without or with a load (useful weight of up to 400 kg). Of course, before the MZM-T was used in a tunnel, the results of the counterweight calculations were verified on a test stand, using specialized software (Figure 17).



Figure 16. The MZM-T on the test stand.

The construction and mass parameters of the manipulator obtained on the basis of the technical documentation made it possible to carry out a simulation that enabled the determination of its movement trajectory and stability [19]. It was assumed that the manipulator would be suspended 4 m from the floor (a_{so}), on the left side of the excavation (Figure 16). For such a system, the movement trajectory of the manipulator tip was determined for the minimum and maximum extensions of the actuators (Figures 18 and 19). It turned out that the manipulator movement capabilities determined analytically were consistent with the research carried out on the test stand, which allowed the support arches (usable weight of up to 440 kg) to be effectively moved to the face, i.e., in front of the roadheader. This eliminated the previous process, where the elements of support arches were provided manually. At the same time, the stability of the boom-counterweight system was determined analytically for the arch transport phase, so that the stabilizing foot did not come into contact with the support. This case was considered in the system of the support, stabilizing the foot (l_{GST}, α_{GST}) and boom, with a maximum rotation of up to 15° and a load

of up to 5 kN. As before, there was no contact between the stabilizing foot and the support, i.e., the model was consistent with the real object (test stand).

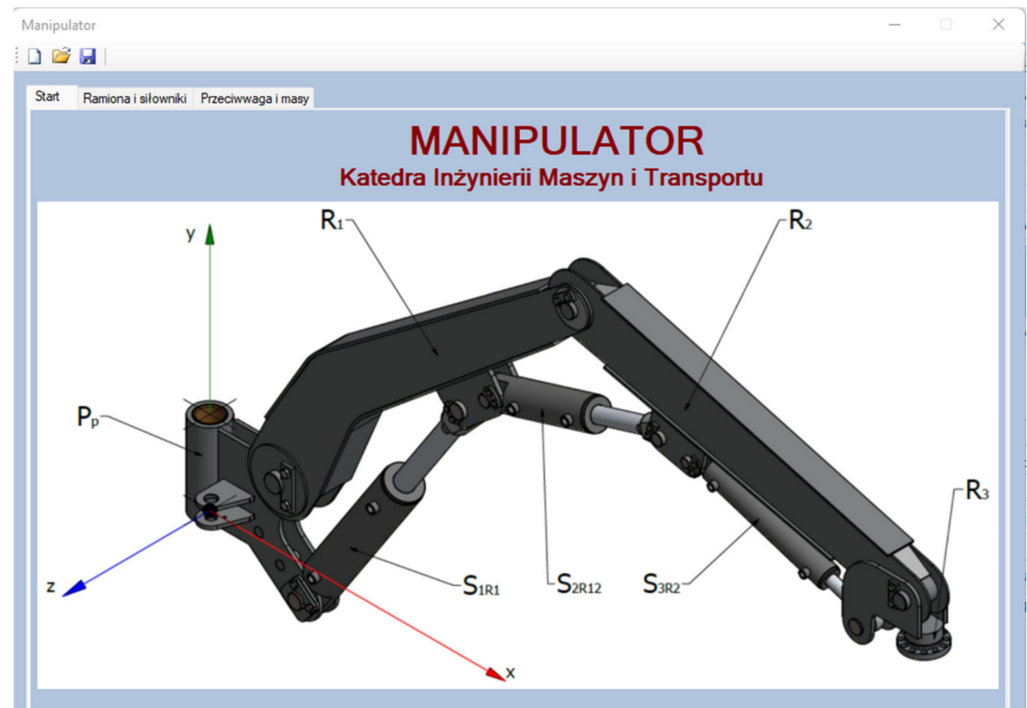


Figure 17. Application page of the program for determining the manipulator's stability.

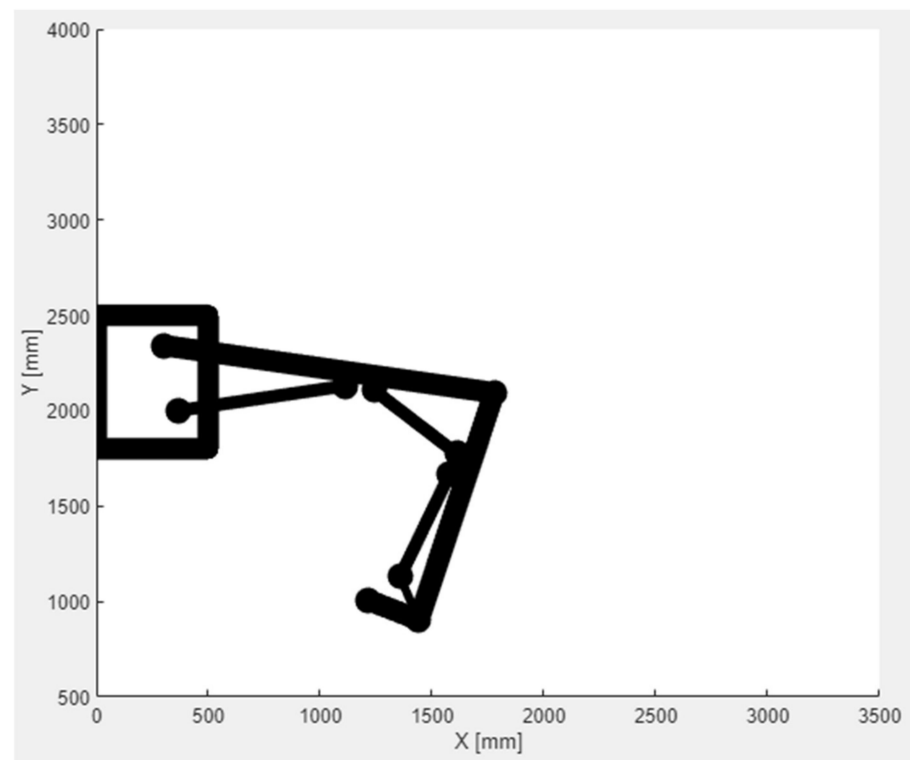


Figure 18. Movement trajectory of the manipulator tip's movement for the minimal extension of the actuators.

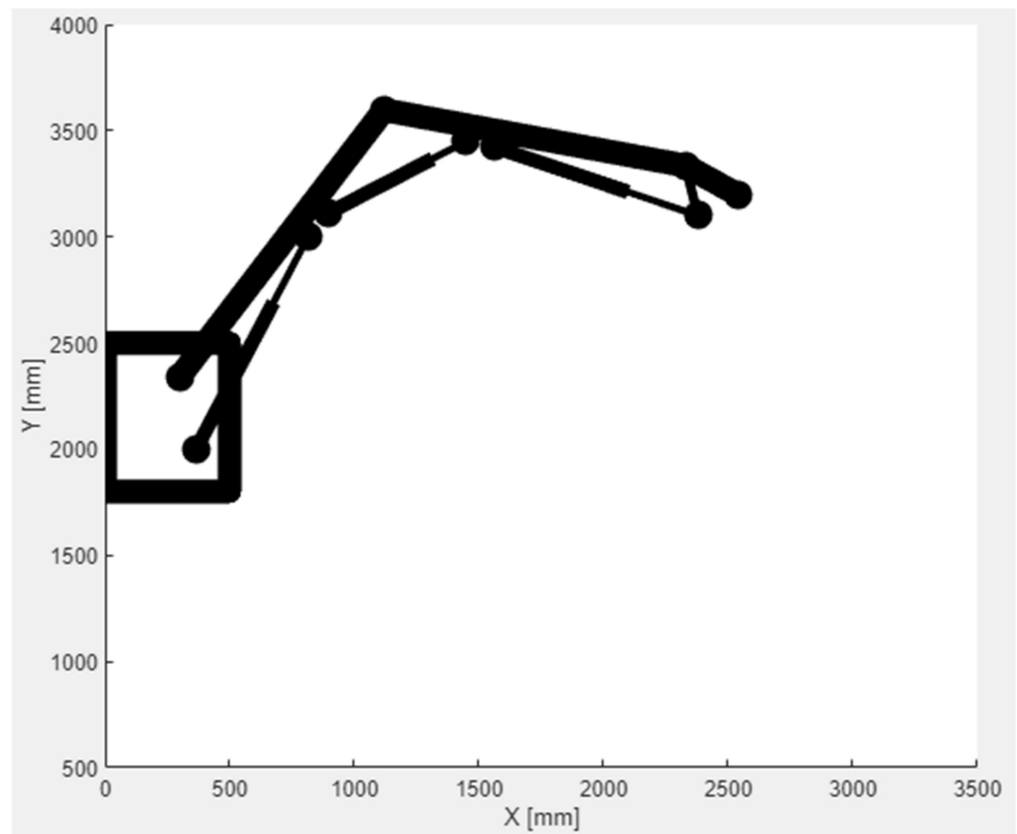


Figure 19. Movement trajectory of the manipulator tip's movement for the maximum extension of the actuators.

4. Conclusions

The aim of developing this manipulator model for supporting assembly works in mining excavations was to describe its basic functions (kinematics, stability) in an analytical way. The model and the calculation results were finally verified in an excavation of a hard coal mine, where the movement capabilities of the manipulator were tested (Figure 20). Given that the design, documentation and working assumptions have been fulfilled, the manipulator can be recommended for practical use in underground workings, and the model and software can be used for design purposes.



Figure 20. View of the MZT-M installed in an underground excavation.

Author Contributions: Conceptualization, K.K., K.M. and T.W.; Data curation, W.H.; Formal analysis, K.K. and R.K.; Funding acquisition, K.K.; Investigation, P.R.; Methodology, K.K.; Project administration, K.M.; Resources, A.K.; Software, T.W. and R.K.; Supervision, K.K.; Validation, R.K. and P.R.; Visualization, T.W.; Writing—original draft, K.K., T.W. and K.M.; Writing—review & editing, K.M. All authors have read and agreed to the published version of the manuscript.

Funding: Works financed by the AGH University of Science and Technology.

Institutional Review Board Statement: Not applicable.

Informed Consent Statement: Not applicable.

Data Availability Statement: Data presented in the article are original and not inappropriately selected, manipulated, enhanced, or fabricated.

Conflicts of Interest: The authors declare no conflict of interest.

References

1. Cao, J.; Zhang, N.; Wang, S.; Qian, D.; Xie, Z. Physical model test study on support of super pre-stressed anchor in the mining engineering. *Eng. Fail. Anal.* **2020**, *118*, 104833. [[CrossRef](#)]
2. Zhu, W.; Xu, J.; Li, Y. Mechanism of the dynamic pressure caused by the instability of upper chamber coal pillars in Shendong coalfield, China. *Geosci. J.* **2017**, *21*, 729–741. [[CrossRef](#)]
3. Xu, Y.; Pan, K.; Zhang, H. Investigation of key techniques on floor roadway support under the impacts of superimposed mining: Theoretical analysis and field study. *Environ. Earth Sci.* **2019**, *78*, 436. [[CrossRef](#)]
4. Małkowski, P.; Ostrowski, Ł.; Bednarek, Ł. The Effect of Selected Factors on Floor Upheaval in Roadways—In Situ Testing. *Energies* **2020**, *13*, 5686. [[CrossRef](#)]
5. Yuan, H.H.; Shan, R.L.; Su, X.G. Deformation characteristics and stability control of a gateroad in fully mechanized mining with large mining height. *Arab. J. Geosci.* **2018**, *11*, 767. [[CrossRef](#)]

6. Mu, W.; Li, L.; Chen, D.; Wang, S.; Xiao, F. Long-term deformation and control structure of rheological tunnels based on numerical simulation and on-site monitoring. *Eng. Fail. Anal.* **2020**, *118*, 104928. [[CrossRef](#)]
7. Tsesarsky, M.; Hatzor, Y. Tunnel roof deflection in blocky rock masses as a function of joint spacing and friction—A parametric study using discontinuous deformation analysis (DDA). *Tunn. Undergr. Space Technol.* **2006**, *21*, 29–45. [[CrossRef](#)]
8. Bednarek, Ł.; Majcherczyk, T. An analysis of rock mass characteristics which influence the choice of support. *Geomech. Eng.* **2020**, *21*, 371–377. [[CrossRef](#)]
9. Cai, M.; Champaigne, D.; Coulombe, J.; Challagulla, K. Development of two new rockbolts for safe and rapid tunneling in burst-prone ground. *Tunn. Undergr. Space Technol.* **2019**, *91*, 103010. [[CrossRef](#)]
10. Wang, Q.; Luan, Y.; Jiang, B.; Li, S.; He, M.; Sun, H.; Qin, Q.; Lu, W. Study on key technology of tunnel fabricated arch and its mechanical mechanism in the mechanized construction. *Tunn. Undergr. Space Technol.* **2019**, *83*, 187–194. [[CrossRef](#)]
11. Xue, G.; Cheng, J.; Guan, J.; Chai, J.; Zhang, G.; Hao, X.; Wu, M. The method for determining working resistance of advance support bracket in deep fully mechanized roadway based on Flac3D. *Adv. Mech. Eng.* **2018**, *10*, 6. [[CrossRef](#)]
12. Wu, K.; Shao, Z.; Qin, S.; Wei, W.; Chu, Z. A critical review on the performance of yielding supports in squeezing tunnels. *Tunn. Undergr. Space Technol.* **2021**, *115*, 103815. [[CrossRef](#)]
13. Rotkegel, M.; Szot, Ł.; Fabich, S. The analysis of selected methods of the yielding of a circular arch support made of V profiles. *Arch. Min. Sci.* **2020**, *65*, 531–550.
14. Horyl, P.; Snuparek, R.; Marsalek, P.; Paczeńskiowski, K. Simulation of Laboratory Tests of Steel Arch Support. *Arch. Min. Sci.* **2017**, *62*, 163–176. [[CrossRef](#)]
15. Nowak, P.; Kilan, Ł. Sandvik experiences with remote controlled machinery. *Min. Inform. Autom. Electr. Eng.* **2019**, *2*, 45–58. [[CrossRef](#)]
16. Korski, J. The efficiency of a bolter miner-requirements and constraints. *Min. Inform. Autom. Electr. Eng.* **2020**, *1*, 37–44. [[CrossRef](#)]
17. Pytlik, A. Tests of steel arch and rock bolt support resistance to static and dynamic loading induced by suspended monorail transportation. *Studia Geotech. Mech.* **2019**, *41*, 81–92. [[CrossRef](#)]
18. Krauze, K.; Bołoz, Ł.; Mucha, K.; Wydro, T. The mechanized supporting system in tunnelling operations. *Tunn. Undergr. Space Technol.* **2021**, *113*, 103929. [[CrossRef](#)]
19. Krauze, K.; Mucha, K.; Wydro, T. Ocena Stateczności Górniczego Manipulatora Transportowo-Montażowego w Różnych Fazach Jego Pracy, a Szczególnie w Czasie Transportu Obudowy do Przdka Wyrobiska Korytarzowego. The Report from re-Search Conducted in the Department of Machinery Engineering and Transport AGH UST 2020, Kraków, Poland. 2020. *unpublished*. (In Polish)
20. Krauze, K.; Mucha, K.; Wydro, T.; Kutnik, A.; Hałas, W.; Ruda, P.; Osowski, D. Operational Tests of a Modular Installation and Transport Assembly of Steel Arch Support in Underground Excavations. In *Multidisciplinary Aspects of Production Engineering—MAPE*; Sitko, J., Ed.; De Gruyter: Warsaw, Poland, 2021; Volume 4, p. 1. [[CrossRef](#)]
21. GTA Roadway Support Machines. Available online: <https://www.gta.eu/en/> (accessed on 3 December 2021).
22. Maas, M. Equipment for underground mining: Projects and new developments at Deilmann-Haniel Mining Systems GmbH. *Min. Rep.* **2014**, *150*, 223–227. [[CrossRef](#)]